SANDIA REPORT
SAND2009-7489
Unlimited Release
Printed November 2009

LDRD Final Report on "Fundamentals of Synthetic Conversion of CO_2 to Simple Hydrocarbon Fuels" (LDRD 113486)

Manos Mavrikakis, Christos T. Maravelias, Constantine A. Stewart, James E. Miller, and Richard A. Kemp

Prepared by
Sandia National Laboratories
Albuquerque, New Mexico 87185 and Livermore, California 94550

Sandia is a multiprogram laboratory operated by Sandia Corporation,
a Lockheed Martin Company, for the United States Department of Energy's
National Nuclear Security Administration under Contract DE-AC04-94AL85000.

Issued by Sandia National Laboratories, operated for the United States Department of Energy by Sandia Corporation.

Available to DOE and DOE contractors from
U.S. Department of Energy
Office of Scientific and Technical Information
P.O. Box 62
Oak Ridge, TN 37831

Telephone: (865) 576-8401
Facsimile: (865) 576-5728
E-Mail: reports@adonis.osti.gov
Online ordering: http://www.osti.gov/bridge

Available to the public from
U.S. Department of Commerce
National Technical Information Service
5285 Port Royal Rd.
Springfield, VA 22161

Telephone: (800) 553-6847
Facsimile: (703) 605-6900
E-Mail: orders@ntis.fedworld.gov
Online order: http://www.ntis.gov/help/ordermethods.asp?loc=7-4-0#online

SAND2009-7489
Unlimited Release
Printed November 2009

LDRD Final Report on "Fundamentals of Synthetic Conversion of CO_2 to Simple Hydrocarbon Fuels" (LDRD 113486)

Constantine A. Stewart, James E. Miller, and Richard A. Kemp
Department 01815 – Ceramic Processing and Inorganic Materials
Sandia National Laboratories
P.O. Box 5800
Albuquerque, New Mexico 87185-1349

Manos Mavrikakis and Christos T. Maravelias
Department of Chemical and Biological Engineering
University of Wisconsin, Madison
Madison, Wisconsin 53706

Abstract

Energy production is inextricably linked to national security and poses the danger of altering the environment in potentially catastrophic ways. There is no greater problem than sustainable energy production. Our purpose was to attack this problem by examining processes, technology, and science needed for recycling CO_2 back into transportation fuels. This approach can be thought of as "bio-inspired" as nature employs the same basic inputs, CO_2/energy/water, to produce biomass. We addressed two key deficiencies apparent in current efforts. First, a detailed process analysis comparing the potential for chemical and conventional engineering methods to provide a route for the conversion of CO_2 and water to fuel has been completed. No apparent "showstoppers" are apparent in the synthetic route. Opportunities to improve current processes have also been identified and examined. Second, we have also specifically addressed the fundamental science of the direct production of methanol from CO_2 using H_2 as a reductant.

ACKNOWLEDGMENTS

We acknowledge the assistance of Mr. Lars Grabow, Mr. Carlos Henao, Mr. Mark Uebel, Ms. Kate Edelman, and Ms. Patricia Nason for experimental and computational help in the carrying out of this project. We also acknowledge the Department of Energy – Basic Energy Sciences Chemical Division for additional funding to aid in the computational work performed and reported in section two.

CONTENTS

FIGURES

TABLES

NOMENCLATURE

DOE	Department of Energy
SNL	Sandia National Laboratories
CO_2	Carbon dioxide
MeOH	Methanol (CH_3OH)
TPD	Temperature programmed desorption
XPS	X-ray photoelectron spectroscopy

1. INTRODUCTION

Energy production, or more precisely the conversion of resources to useful forms of energy, is the largest human enterprise on the planet. As such, it is inextricably linked to national security and quality of life, but also poses the danger of altering the environment in potentially catastrophic ways. Thus, there is no greater problem than sustainable energy production. Sandia scientists are just beginning to attack this problem in new ways by developing processes and technology for recycling CO_2 back into liquid transportation fuels, thus helping to ensure domestic and battlefield energy supplies as well as mitigate global climate change. This approach can be thought of as "bio-inspired" as nature employs the same basic inputs, CO_2/energy/water, to produce biomass.

Along with the production of energy, another major issue facing humankind is the rise in levels of CO_2 in the atmosphere. The extent of global warming that can be attributed solely to the rise in CO_2 levels is debatable; however, that these CO_2 levels do affect climate change to some degree cannot be denied. To alter the level of CO_2 in the atmosphere is a massive technological undertaking. Producing chemicals from waste CO_2 is admirable, but the extent of CO_2 reduction in a chemicals-only scenario is not great, due to the small volumes of chemicals derived form CO_2. However, recycling CO_2 via some type of reductive process to regenerate transportation fuels, or a suitable fuels precursor, does have the volume necessary to reduce or stabilize CO_2 levels in the atmosphere. As well, generating fuels from a non-crude oil source also aids in the economic stability and security of the United States.

CO_2 is an energy-depleted molecule – the conversion of a hydrocarbon to CO_2 and H_2O is a significantly downhill, exothermic process. In order to return this oxidized molecule to a usable fuel, it must be converted (reduced) back into a suitable precursor. In order to do this, one can use electrons (electrochemistry) or an appropriate reducing agent such as H_2. In the work discussed in this report, we assume that the reducing agent is H_2, most likely eventually derived from photo-splitting of water.

Herein, we have addressed two key deficiencies that have become apparent as work proceeds in other laboratories. First, prior to our work a detailed process analysis comparing the potential for nanotechnology and conventional engineering methods, *e.g.*, in the form of catalysts and active materials in a chemical plant environment, to provide a viable route for the conversion of CO_2 and water to fuel, to that provided by nature, *i.e.*, biomass, had not been completed. Understanding the possible advantages and/or disadvantages of the two routes is a key to establishing credibility as well as to identifying key hurdles and the most fruitful directions for research. Also, it is critical to understand whether there are any "showstoppers" or serious technical hurdles in the synthetic routes. This topic will be covered in the first section of this SAND report. Second, we more specifically address the science of applying nanotechnology to the direct production of methanol from CO_2, either

chemically or electrochemically, using water, or H_2 derived from water, as a reductant. In particular, the use of density functional theory (DFT) to examine the fundamental steps in the conversion of CO_2 into a small organic molecule, methanol, has been performed. Interactions of CO_2 with the Cu surface present in heterogeneous catalysts have been studied. The second part of this report will cover the theoretical aspects of our team's studies. Another aspect of our work that was performed in conjunction with the University of Texas in the area of metal nanoparticles grown within an electrically-conducting polymer matrix will be covered in another SAND report when complete, and as such those results are not reported here.

2. SYNTHETIC PRODUCTION OF METHANOL – PROCESS ANALYSIS

2.1 Section Summary

Energy security and global climate change are two intertwined problems that demand attention. The vision for the "hydrogen economy" is a proposed solution that is based on the application of sustainable energy sources to split water. However, many technical and infrastructure challenges remain for hydrogen that do not exist for hydrocarbon fuels. Integrating CO_2 capture and conversion into liquid fuels produces a new vision that promises the benefits of hydrogen while preserving many of the advantages of the hydrocarbon economy. In this section, we study the production of methanol from H_2/CO_2 and H_2O/CO mixtures. We present two alternative processes that are based on the combined action of two reversible reactions: water gas shift (WGS) and methanol synthesis (MS) on a $Cu/ZnO/AlO_3$ catalyst. Detailed flowsheet simulations and economic evaluations under multiple scenarios indicate that both processes can be economically feasible in the near future, while having energy efficiencies that are significantly better than their biological counterpart. Finally, the conversion and energy efficiency of both processes are better than previously proposed designs such as the so-called CAMERE process.

2.2 Introduction

Energy resources are the foundation for developed economies and are inextricably linked to national security, social stability, and quality of life. Hence, global demand and competition for petroleum as a transportation fuel is projected to continue to climb even as supplies of conventional oil decline. Less-conventional resources such as coal, oil-shale and tar-sands can be converted to liquid fuels and help fill the gap. However, tapping into and converting these resources into liquid fuels exacerbates green house gas emissions as they are carbon rich, but hydrogen deficient. Revolutionary thinking is required if the coupled problems of energy (transportation) security and climate change are to be addressed. Hydrocarbon fuels are ideal energy carriers, but they can no longer be thought of as primary energy sources. Rather, it is necessary that we take the realistic view that our conventional hydrocarbon fuels are in fact "stored sunlight" and "sequestered carbon." That is, petroleum, coal and other fossil fuels are the end result of a long process that began with a biological organism capturing sunlight and using it to drive chemical conversions of CO_2 and H_2O to hydrocarbons and oxygen (photosynthesis).

Biofuels, *e.g*. bio-ethanol, can be thought of as a modern approach to improving upon the overall (sunlight to fuel) efficiency of this process and shortening the time scale. As before, the starting point is the photosynthetic conversion of CO_2 and H_2O to hydrocarbons. Additional chemical or biological steps are then undertaken to produce a hydrocarbon fuel. The overall sunlight to fuel efficiency is dependent on location and the process specifics and is thus difficult to define precisely or to generalize. However, it is still generally quite low, although significantly better than that for oil. As an example, it is commonly accepted that the solar to ethanol efficiency from corn kernels is less than 1% [1]. One can put an upper limit on the biomass approach by considering the efficiency of the photosynthetic step alone. Photosynthesis is generally measured to be 2.5% efficient at best [2]. The maximum possible efficiency is estimated to be 4.6% for C3 photosynthesis and 6% for C4 photosynthesis, under current atmospheric conditions [3].

Given the limits on overall sunlight to hydrocarbon efficiency imposed by photosynthesis, it is reasonable to consider other, more direct, chemical approaches for "re-energizing" CO_2 and H_2O and ultimately converting them to transportation fuels. Solar-driven thermochemical processes have the potential to split CO_2 and H_2O to yield CO and H_2 at high solar efficiencies [4, 5]. In this paper we consider two process alternatives for converting the products of this and similar processes to methanol, as starting point for determining the viability of this approach. We consider methanol because it can be converted to liquid fuels and chemicals, and used in direct methanol fuels cells.

2.3 Process Alternatives

The first process converts H_2 and CO_2 into methanol (70,000 MT_MeOH/yr), while the second one converts CO and H_2O into methanol (85,000 MT_MeOH/yr). All reactors in this study are multi-tube packed with a commercial $Cu/ZnO/Al_2O_3$ catalyst.

2.3.1. Process Alternative #1: Methanol from H_2 and CO_2

The proposed process includes two reaction systems and one separation system. In the first reaction system H_2 and CO_2 are partially converted according to the reaction:

$$H_2 + CO_2 \leftrightarrow H_2O + CO \qquad \text{Reverse WGS (RWGS)}$$

After removing most of the produced water, the resulting $H_2/CO_2/CO$ mixture is then fed to a second reaction system where two reactions take place:

$$CO_2 + 3H_2 \leftrightarrow CH_3OH + H_2O \qquad \text{Methanol Synthesis (MS)}$$

$$CO + H_2O \leftrightarrow CO_2 + H_2 \qquad \text{Water Gas Shift (WGS)}$$

The purpose of the first reaction system is to produce enough CO to eliminate, via WGS, the water produced by MS. This is beneficial because water has been proven to block active sites in the MS catalyst. The separation system consists of a distillation column to separate the heavy products methanol and water.

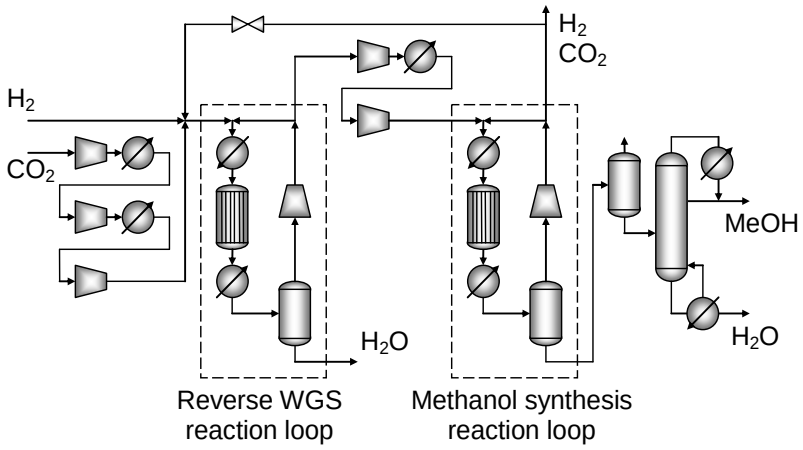

Figure 1. MeOH Production from H_2 and CO_2.

The flowsheet of this process is shown in Figure 1. It is an improvement over the CAMERE processes [6]. The main difference between this alternative and the original CAMERE process is the presence of the recycle loop from the exit of the second reactor to the entrance of the first. The optimization of the reactor conditions and major recycle streams leads to a significant improvement of the overall H_2-to-methanol yield, from 53% in the original CAMERE process to 87%.

2.3.2. Process Alternative #2: Methanol from H_2O and CO

In this case, H_2O and CO coming from the thermo-chemical splitting of CO_2 are converted to methanol in the process shown in Figure 2. As in the previous case, this alternative includes two reaction systems. In the first one, H_2O and CO are partially converted according to the reaction:

$$H_2O + CO \leftrightarrow H_2 + CO_2 \qquad \text{Water Gas Shift (WGS)}$$

The resulting $H_2/CO/CO_2$ mixture is then passed to an absorption system which selectively removes part of the CO_2, adjusting the CO/CO_2 ratio before feeding it to the second system where methanol is produced according to:

$$CO_2 + 3H_2 \leftrightarrow CH_3OH + H_2O \qquad \text{Methanol Synthesis (MS)}$$

$$CO + H_2O \leftrightarrow CO_2 + H_2 \qquad \text{Water Gas Shift (WGS)}$$

The purpose of the first reactor is to produce enough H_2 and CO_2 to drive the production of methanol in the second reactor, while leaving enough CO to eliminate the poisoning from the produced water.

There are some fundamental differences between the two alternatives. First, the CO_2 used in the methanol synthesis is not fed to the process, but produced by partial transformation of the CO feed. Second, the control of the CO/CO_2 ratio is achieved by an additional separation system. Note that in the integrated process this separation system will be used for the recycling of CO_2 back to the thermochemical splitting reactor.

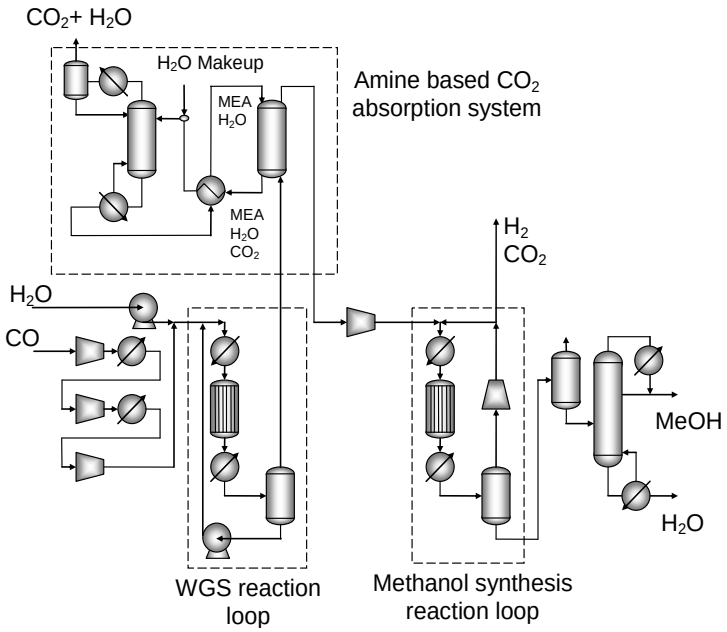

Figure 2. MeOH Production from H_2O and CO_2.

2.3.3. Conversion and Energy Efficiency

The two processes were modeled in ASPEN PLUS®. Some of the most important characteristics of the two alternatives are presented in Table 1. The H_2, CO to MeOH yields are based on the stoichiometry of the combined reactions discussed earlier (*i.e.* $CO_2 + 3H_2 \rightarrow MeOH + H_2O$ for the first process, and $3CO + 2H_2O \rightarrow MeOH + 2CO_2$ for the second process). In this study, the energy efficiency is defined as the ratio of the energy released by burning the produced MeOH, and the total energy that enters the process as chemical energy in the main raw material (reenergized H_2O in the form of H_2 or reenergized CO_2 in the form of CO) plus the energy supplied by the utility system.

Table 1. Major Process Characteristics

Process alternative	1	2
Material flows [kmol/h]:		
H_2	900	--
CO	--	1050
MeOH	262	323
Capacity (MT_MeOH/yr)	70,000	85,000
H_2 to MeOH yield	87%	--
CO to MeOH yield	--	92%
Reactor #1 T-P [°C]-[bar]	310 - 15	270 - 22
Reactor #2 T-P [°C]-[bar]	240 - 46	205-46
Reactor catalysts	$Cu/ZnO/Al_2O_3$	$Cu/ZnO/Al_2O_3$
Energy efficiency	49%	62%

2.4 Economic Evaluation

Detailed economic evaluation of both process alternatives was conducted using ICARUS PROCESS EVALUATOR® based on the detailed process simulation models, and the evaluation parameters given in Table 2.

Table 2. Economic Evaluation Parameters.

Project's Economic Life [yr]	30
Working Capital/Capital Expense	5%
Operating Charged /Operating Labor	15%
Plant Overhead/Operating Labor	40%
Desired Rate of Return[%/yr]	8%
Tax Rate[%/yr]	40%
Salvage Value/Capital Cost	20%
Depreciation	Straight line
Capital Escalation [%/yr]	5%
Raw Material Escalation [%/yr]	1.5%
Product Escalation [%/yr]	5%
Utility Escalation [%/yr]	3%

The main objective of this analysis was to determine the break-even prices of H_2 and CO that would allow the processes to be economically feasible. In order to accomplish this, prices of CO_2, H_2O and MeOH according to recent technology analysis and market trends were used. Detailed Net Present Value (NPV) sensitivity analysis studies were also performed for both projects. Material prices were selected as follows:

- CO_2 price: Several studies identify amine absorption as one of the most economic systems for CO_2 sequestration [7]. Using this technology the price of CO_2 coming from a sequestration unit in a power station is around 35 USD/tonCO_2.
- H_2O price: The price considered here was the standard value of de-ionized water: 1 USD/MTon.
- Methanol price: Methanol price has a highly fluctuating behavior. For this particular study, the most recent value 330 USD/MT was considered (www.methanex.com).

The capital expenditure for both projects were around 17.5 million USD. The NPV sensitivity analysis studies indicate that the maximum raw material prices are 1.12 USD/kgH_2 for process #1, and 0.17 USD/kgCO for process #2 (see Figures 3 and 4). However, even if the prices are as high as 2.2 USD/kgH_2 and 0.275 USD/kgCO, respectively, both processes can still be economically viable if the price of methanol is around 550 USD/MT (see Figure 5), which was the price of methanol as per Sept 2008. Note that the price of methanol is expected to increase in the future reaching at least 500 USD/MT.

Furthermore, in the current study we assumed that we pay 35 USD/tonCO_2 for sequestration. However, if emission regulations or emission trading schemes are introduced, CO_2 consumers will get credits, which means that the NPV of process #1 will increase.

Finally, we carried sensitivity analysis studies that show that an improvement of less than 5% in the overall yield of H_2 and CO in processes #1 and #2, respectively, have a substantial impact on the profitability of the two processes. Therefore, we believe that research efforts in the area of new catalyst development and process optimization will result in significant improvements. We are currently working towards these two goals, as well as the development of an integrated process that includes the thermochemical splitting of CO_2 and the conversion of CO/H_2O to methanol.

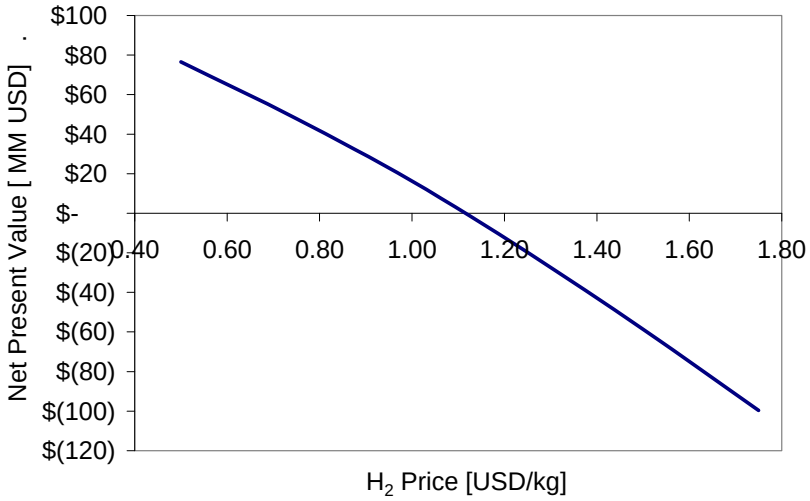

Figure 3. Effect of H_2 Price on Process#1 NPV.

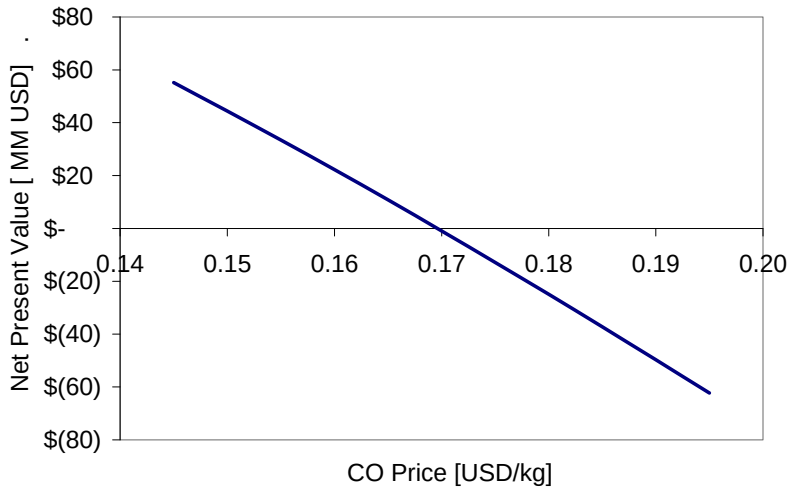

Figure 4. Effect of CO Price on Process#2 NPV.

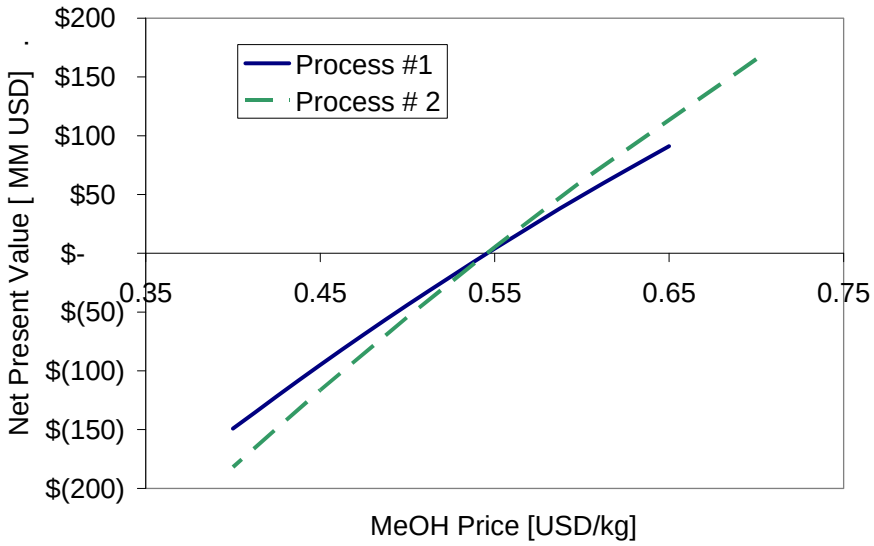

Figure 5. Effect of MeOH price on NPV, assuming H_2 price = 2.5 USD/kg and CO price = 0.275USD/kg.

2.5 Conclusions

We presented two process designs for the production of methanol from H_2/CO_2 and H_2O/CO. The two alternatives can be integrated with thermochemical processes for the splitting of H_2O and/or CO_2, leading to technologies that can change the way we view renewable energy. The integrated processes satisfy the twofold objective of fomenting the use of renewable energy (in this case concentrated solar power) while reducing CO_2 emissions trough recycling. Simulations of the proposed alternatives feature methanol yields significantly better than those reported in the literature. Based upon current methanol prices, sensitivity analysis indicates economic feasibility, if prices do not exceed 1.12 USD/kgH_2 (7.88 USD/GJ) and 0.17 USD/kgCO. However, even if the cost is twice as high, the processes can be economically attractive if the price of methanol increases moderately.

3. INTERACTION OF CO_2 WITH COPPER OVERLAYERS

3.1 Introduction

3.1.1. Carbon Dioxide Chemistry

The importance of CO_2 chemistry on copper surfaces in connection with methanol synthesis and the water-gas shift reaction is well-established. Methanol is synthesized from a mixture of CO, CO_2, and H_2, with CO_2 hydrogenation being the major pathway [8]. Isotope labeling experiments have shown CO_2 to be the source of carbon in methanol formation [9-11].
Extensive reviews regarding the surface chemistry of carbon dioxide on several metals have been published by Solymosi [12], and by Freund and Roberts [13]. CO_2 physisorbs on most transition metals. Evidence for significant interaction has only been found for stepped and rough copper surfaces [14, 15] and in connection with alkali doping or by co-dosing oxygen [16-18].

Several studies have examined the reactivity of CO_2 with the low index Cu surfaces Cu(111), Cu(110), and Cu(100). Habraken *et al.* [19] observed no interaction of CO_2 with a clean or an oxygen covered Cu(111) surface at 297 and 637 K with exposures up to 5×10^5 L, and Campbell *et al.* [20] found very slow dissociation of CO_2 on Cu(111) at 50 torr and 490 K. Rodriguez *et al.* [16] employed doses of up to 350 L on a Cu (110) surface at 110 and 250 K, but were also unable to dissociate CO_2. Similar studies on the Cu(110) surface by Fu and Somorjai [14], Krause *et al.* [21], Ernst *et al.* [22], and Funk *et al.* [23] found no reaction at low temperature and CO_2 doses. In stark contrast to these observations, Wachs and Madix [24] reported that 99 % of the adsorbed CO_2 on a Cu(110) crystal dissociated into CO and surface oxygen, but unfortunately the pressure and temperature applied were not stated. Moreover, Schneider and Hirschwald [25] reported dissociation on this surface. These results have, however, been disputed, and the reactivity may have been due to surface defects [22, 26, 27]. Except for the two anomalous results discussed above, dissociative adsorption on low index Cu surfaces has only been found at temperatures above 400 K and at pressures of several mbar [20, 28, 29]. Nakamura *et al.* [29] established that high pressure was required for the reaction to occur on Cu(110), and similarly CO_2 was observed to dissociate on Cu(100) under high pressure (900 mbar) by Rasmussen *et al.* [28]

Except for a study by Carley *et al.* [18], who observed that adsorbed carbonate (CO_3) could be formed by co-adsorbing oxygen with CO_2 on Cu(110), stabilization of CO_2 has not been observed on low index Cu surfaces. A different scenario is found on the higher index and rough copper surfaces where reactivity is enhanced. The dissociation to carbon monoxide and oxygen occurs under UHV conditions for Cu(311) at 150 K [14] and for Cu(332) at 95 K [15]. Studies of polycrystalline Cu [30-32] have also revealed CO_2 dissociation, although photo-induced reactions should in some cases be considered [32, 33].

A number of studies on stepped single crystal surfaces [15], polycrystalline Cu samples [34], and industrial $Cu/ZnO/Al_2O_3$ catalysts [35, 36] have speculated or observed that carbonate species are present on the surface during reaction. It is clear that additional studies are needed that can provide further insight into the interaction of CO_2 with copper surfaces.

3.1.2. The Cu/Pt(111) System

The industrial catalyst for methanol synthesis and the low temperature water-gas shift reaction is comprised of nano-sized copper clusters supported on zinc oxide and aluminum oxide ($Cu/ZnO/Al_2O_3$). In spite of a great number of studies, the nature of the active sites in methanol synthesis and the role of the ZnO-support are still subjects of debate. Topsøe and Topsøe found that the active copper species during synthesis is metal-like and that varying reducing conditions influence the nature of the Cu surfaces in Cu/ZnO reversibly, including the formation of a CuZn surface alloy at severe reducing conditions [37]. Further support of these notions has been provided by the results of density functional theory (DFT) calculations [38].

Microkinetic modeling of the water-gas shift reaction has suggested that the activity of copper-based catalysts can be improved by increasing the bonding energy of both carbon monoxide and atomic oxygen to the surface [39]. Ways to achieve this include stretching of the Cu lattice and introduction of low coordination sites. This will result in a narrowing of the d-band due to a larger nearest neighbor distance, and as the degree of filling must be preserved, the d-band will shift up. This results in a stronger bonding of the adsorbates and higher reactivity [40-44]. It is therefore interesting to examine the interaction of CO_2 with a well-defined model system that can emulate both stretching of the Cu lattice and roughness. A bimetallic system that possesses the required properties is copper deposited pseudomorphically on platinum, as the lattice spacing for Cu(111) is 8 % smaller than that of Pt (111) leading to a strained Cu overlayer.

Cu/Pt(111) has been thoroughly investigated experimentally[40, 45-56] and theoretically[40, 41, 57, 58] during the last three decades. Scanning tunneling microscopy (STM) and He atom scattering (HAS) have revealed that the growth of copper is 2D-pseudomorphic with nucleation at the step sites of the Pt surface [52]. At room temperature, two-dimensional dendritic Cu islands are formed and grow from the step edges coalescing into a defective pseudomorphic overlayer as coverage increases. The second layer commences growth before the first is complete and is rotationally commensurate to the Pt substrate with a lattice parameter closer to that of bulk Cu(111) [48]. Holst *et al.* [52, 53] examined the structure of Cu on Pt(111) at different deposition temperatures. No reconstruction was observed at 340 K, but a highly defective surface was grown. Higher deposition temperatures yielded smoother

overlayers. At 450 K a reconstruction that was assigned to take place in the Pt substrate was observed.

A Cu/Pt near surface alloy has recently received attention as a possible water-gas shift catalyst [58]. AES data [47] and work function measurements [48] suggest that alloying sets in around 550 K. Unfortunately, no ISS studies have been conducted except for Cu deposited on the vicinal Pt (12 12 11) facet where the onset of surface alloying is found above 350 K [59]. A steady dissolution of Cu into the bulk is obtained upon heating [56], and at temperatures above 1350 K the Cu will move out of the Pt bulk and evaporate [60]. The Cu/Pt system has mainly been probed using oxygen [54, 55], hydrogen, and CO [46, 48, 49, 51]. To our knowledge, no studies have employed high-pressure conditions or examined the interaction of CO_2 with Cu/Pt surfaces.

3.2 Methods

3.2.1. Experimental

The setup used is an ultra-high vacuum chamber with a base pressure of about 1×10^{-10} torr. The chamber is connected to a high-pressure cell (HPC) as described in Ref. [61], and is separated from the UHV chamber with a lock that utilizes a Cu-gasket [62]. The chamber is equipped with standard UHV surface science techniques such as x-ray photoelectron spectroscopy (XPS), ion scattering spectroscopy (ISS), electron energy loss spectroscopy (EELS), low energy electron diffraction (LEED), and a differentially pumped quadrupole mass spectrometer for temperature programmed desorption (TPD).

It is possible to introduce a pressure of several bar in the HPC and to conduct in-situ polarization modulation infrared reflection absorption spectroscopy (PM-IRRAS) [63-65], an FT-IR method which utilizes different polarizations of the radiation to distinguish between adsorbates on the sample surface and the gas phase. P-polarized radiation orthogonal to the surface can be absorbed by vibrational excitation of surface species whereas the parallel s-polarized radiation cannot. The signal is the difference between the reflectivities of the two polarizations normalized with their sum. The infrared source and interferometer is a Nexus spectrometer supplied by Thermo Nicolet, and the photoelastic modulator and demodulator have been supplied by Hinds Instruments and GWC Technologies. ZnSe windows have been fitted onto the HPC in order to allow transmission of the beam. The radiation is then reflected off the sample with an angle of incidence between the beam and the crystal surface of 82° and is focused onto a MCT (HgCdTe) detector cooled with liquid N_2. The photoelastic modulator (PEM) and demodulator use a modulation frequency in the 100 kHz range and the optical material of the modulator is ZnSe. The lenses, polarizer, modulator, and detector outside the Nexus module are all exposed to air, and absorption bands from water and CO_2

are present in the unmodulated spectra, but not in the PM-IRRAS demodulated spectra. A dehumidifier and filter is fitted to the system to minimize these absorption bands.
The sample is a platinum single crystal supplied by Metal Crystals & Oxides Ltd. cut in the (111) direction. It was cleaned using cycles of oxygen exposure of 10^{-6} mbar at 850 K, sputtering with Ar, and annealing at 1270 K. This was repeated until no impurities were detected with XPS and ISS.

Cu overlayers on Pt(111) were prepared by physical vapor deposition with a rate of approx. 0.2 ML/min at a substrate temperature of 425 K. The CuPt surface alloy with a Cu/Pt ratio of 1:2 investigated in this work was prepared by annealing 1 ML Cu on Pt(111) briefly to 573 K. All samples were characterized by XPS and ISS.

N48 grade CO_2 was purified further with several freeze-pump-thaw cycles using liquid nitrogen, before it was let into the HPC at room temperature. Cleanliness was checked by exposing the Pt(111) crystal to 0.5 bar CO_2. No adsorbed oxygen was subsequently observed with XPS other than CO adsorbed from the background pressure of the chamber. Unless otherwise stated, the sample was subjected to 0.5 bar CO_2 at room temperature.

3.2.2. Theoretical

CO_3 adsorption was examined on a variety of Cu, Pt, and Cu/Pt alloy surfaces using the DACAPO total energy code [44, 66]. The specific systems studied were Cu(111), Pt(111), 1 ML Cu on Pt(111) (overlayer), Pt-Cu-Pt(111) (sandwich), and Cu/Pt 1:1 mixed overlayer on Pt(111). For all systems both the (111) surface on (2×2) and (3×3) unit cells, and the (211) facet on a (3×2) unit cell were studied. The only exception was the Cu/Pt 1:1 mixed overlayer, where only (111) surfaces were examined. Convergence with respect to **k**-point set, surface relaxation, and number of atomic layers was tested. Converged results are obtained for 4 layer slabs with the top 2 layers relaxed and 54 or 18 Chadi-Cohen **k**-points for (111) facets of slabs containing Cu and pure Pt systems, respectively. For the stepped (211) facets we employed a 4×4×1 Monkhorst-Pack **k**-point grid.

CO_3 frequencies were calculated using the harmonic oscillator assumption by diagonalization of the Hessian matrix obtained with a displacement of 0.01 Å [67]. Relative intensities were estimated based on dipole changes. Special care was taken to project the dipole change onto the same direction as in the experimental setup; for instance, for the (211) surfaces, the dipole change is projected onto the vector perpendicular to the (111) terraces. Hence, IR selection rules apply.

3.3 Results and Discussion

3.3.1. Characterization of the Cu/Pt System

The Cu coverage was determined by comparing ISS and XPS data sets for different deposition times at a substrate temperature of 425 K, see Figure 6. ISS intensities for Cu were normalized with the sum of the Pt and Cu intensities, and Cu 2p XPS signals were normalized to Pt 4f. In effect, matters are complicated by the growth of the second layer before the first layer is complete. LEED images (not shown) revealed the emergence of weak rosette patterns around the main first order Pt spots for 0.6 ML Cu indicating onset of second layer formation around this point. The deposition rate of Cu was determined using a linear fit of data points up to 0.6 ML coverage, where ISS spectra are expected to represent the coverage fairly well. The amount of Cu above this point was then estimated on the basis of the deposition rate as it was concluded that the XPS signal intensity for the Cu 2p doublet would be a poor estimate due to island formation. It is noted that the normalized XPS signal in Figure 6 seems to have a value different from zero when no Cu ISS signal is present. An explanation may be that alloying is occurring at the Pt steps at the early stages of growth.

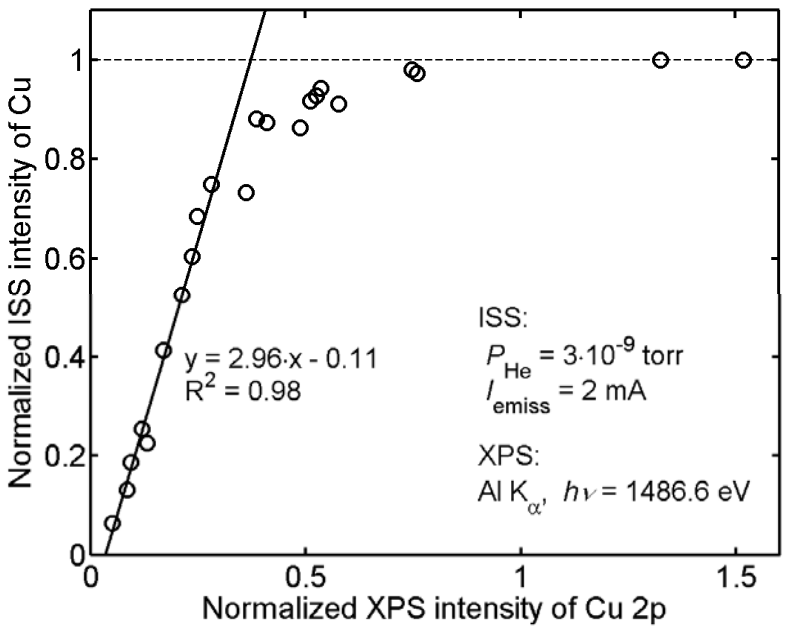

Figure 6. Intensity of Cu signal in ISS versus intensity of Cu 2p doublet from XPS for several deposition times. For XPS Cu signals were normalized against the Pt 4f signal. A linear fit to all data points up to an ISS signal of 0.6 is shown.

The dendritic growth of the copper islands from the platinum steps and uncompleted coalescence seen with STM[52, 53] together with the LEED patterns from the present study, point to a highly defective surface. For 1 ML Cu deposited at 425 K, extensive second layer growth is found as clear rosettes around the first order spots are observed in LEED. Surface defects, steps, and kinks should hence be abundant, and it is clear that defects may dominate reactivity at this coverage. Furthermore it cannot be excluded that intermediates may induce a reconstruction of the Cu layer during reaction. STM studies of the Cu/Pt(111) system with intermediates would be needed to investigate this scenario further.

The onset of surface alloying was determined by heating the sample from 350 K to 600 K with 1 ML Cu in intervals of 50 K from 350 K to 450 K and in steps of 10 K above 450 K. For each step an ISS spectrum was taken keeping the sample at the selected temperature for 1 min, see Figure 7. For data comparison, the same sample was used throughout the experiment. Several precautions were taken to minimize sputter effects, *e.g.*, lowering of He pressure and emission current, together with an increase of the area rastered, while still maintaining an adequate signal. An emission current of 2 mA, a pressure of 3×10^{-9} mbar, and a primary energy of 1180 eV were employed. In order to estimate the removal of Cu caused by the small amount of sputter damage during ISS the decrease in intensity of the first three measurements at low temperature was determined and compared to the observed changes in the following measurements. This did not change the result evident from the figure that surface alloying sets in at 460 K. This temperature is quite low compared to other studies of the Cu/Pt system, where alloying around 525-550 K have been reported from AES, LEED, and work function measurements [47, 48, 56]. Our result is, however, similar to the before mentioned onset of a reconstruction of the Pt surface which was also evident in the Cu overlayer as seen with STM [53]. Further increase in temperature merely leads to a higher rate of Cu migration into the Pt bulk [56].

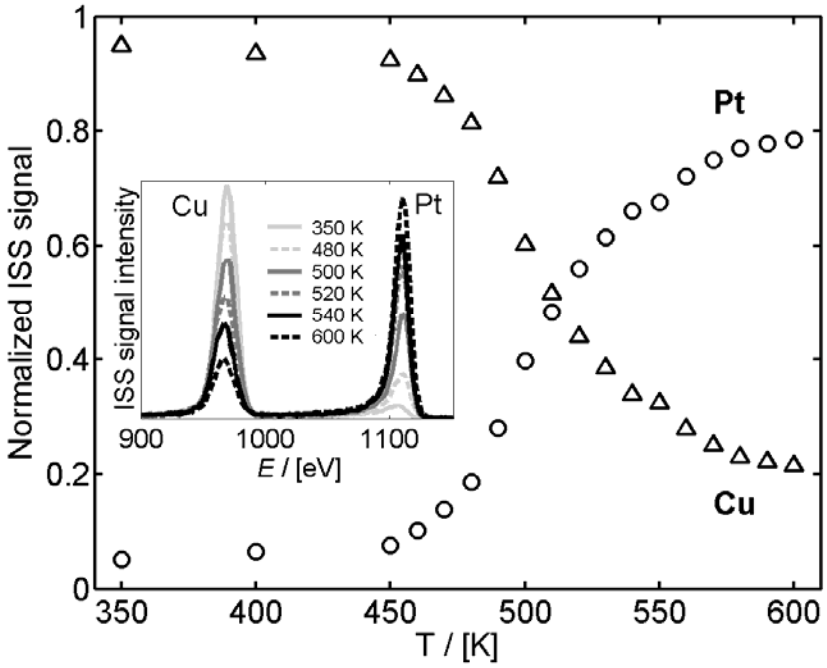

Figure 7. Normalized ISS intensities of Cu and Pt measured after heating in intervals of 50 K from 350 K to 450 K, and in 10 K steps between 450 K and 600 K. Inset shows ISS spectra acquired at 350 K, 480 K, 500 K, 520 K, 540 K and 600 K.

3.3.2. Vibrational Spectroscopy Results

Cu overlayers from 0.4 ML and up to 5.5 ML were subjected to high pressures of CO_2 at room temperature. PM-IRRAS spectra recorded at pressures ranging from 550 mbar down to 10 mbar for 1 ML Cu are shown in Figure 8. A sharp, strong feature was seen at 1435 cm^{-1} similar to results from Millar *et al.* on Cu/SiO_2 [68]. With pressure decreasing that feature was shifted down in energy to 1410 cm^{-1} and disappeared when the CO_2 had been pumped out. A stationary feature that persisted in vacuum at 1315 cm^{-1}, and a weak peak at 1215 cm^{-1} – 1205 cm^{-1} (not shown) that presented behavior similar to the 1435 cm^{-1} feature, were also identified.

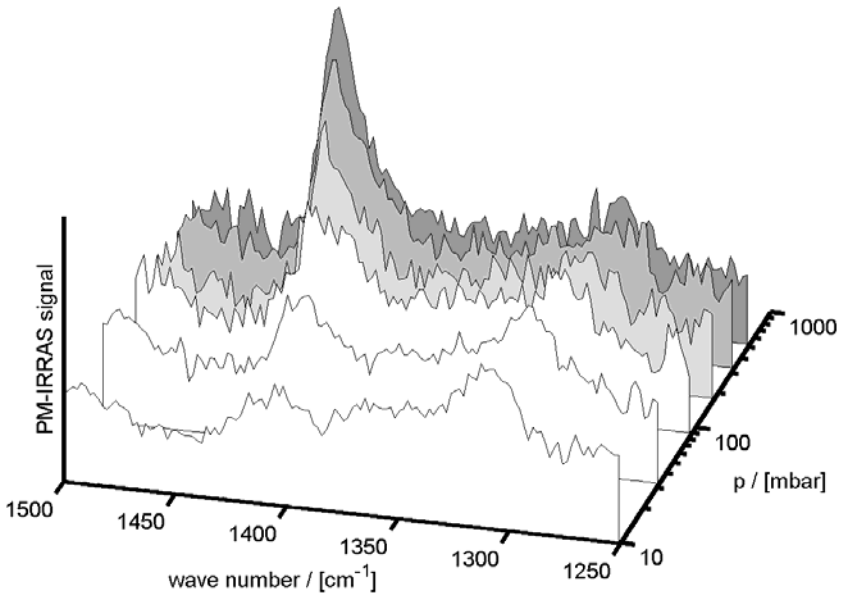

Figure 8. PM-IRRAS spectra in the range 1250 – 1500 cm^{-1} for 1 ML Cu taken at CO_2 pressures ranging from 550 mbar down to 10 mbar. The high pressure was applied first, and then the pressure was gradually lowered.

Subsequent EELS spectra showed peaks at approx. 280, 820, 1050, and 1300 cm^{-1}, see Figure 9, where the vibration at 1300 cm^{-1} is identical to the one seen in IRRAS. The features observed are broad because of the low resolution of the EELS equipment. Despite extensive optimization it was not possible to obtain a FWHM smaller than 19 meV. The vibrations identified here are very similar to those reported in studies done by Stuve *et al.* on the interaction of CO_2 with an Ag (110) single crystal predosed with oxygen [69]. They assigned the vibrations to the metal–O stretch, ν(M-O), the out-of-plane CO_3 deformation, $\pi(CO_3)$, the C-O stretch, ν(CO), and the symmetric O-C-O stretch, ν_s(O=C=O), respectively. This ensemble of vibrations suggest that the carbonate is lying nearly flat on the surface, as the out-of-plane deformation where the carbon atom moves back and forth through the plane described by the oxygen atoms is seen. None of the vibrations observed at high pressure or under UHV conditions are from adsorbed CO_2, see Table 3.

Table 3. Observed vibrational frequencies in cm^{-1} compared to results from Stuve *et al.* [69] together with their assignments.

Assignments from Stuve *et al*. [69]	CO_2 Gas [70] as referenced in Ref. [69]	Adsorbed, Ag [69]	CO_3 Adsorbed, Ag [69]	Adsorbed, Cu/Pt This work
ν(M-O)	-	-	270	280
Bend, δ(O=C=O)	667	660	-	-
$\pi(CO_3)$	-	-	850	820
ν(CO)	-	-	1050	1050
δ(O=C=O) overtone	1286	1280	-	-
ν_s(OCO)	-	-	1360	1310
Sym. str., ν_s(O=C=O)	1388	(1390) Hidden by 1360 cm^{-1} peak	-	-
Asym. str. ν_a(O=C=O)	2349	2350	-	-

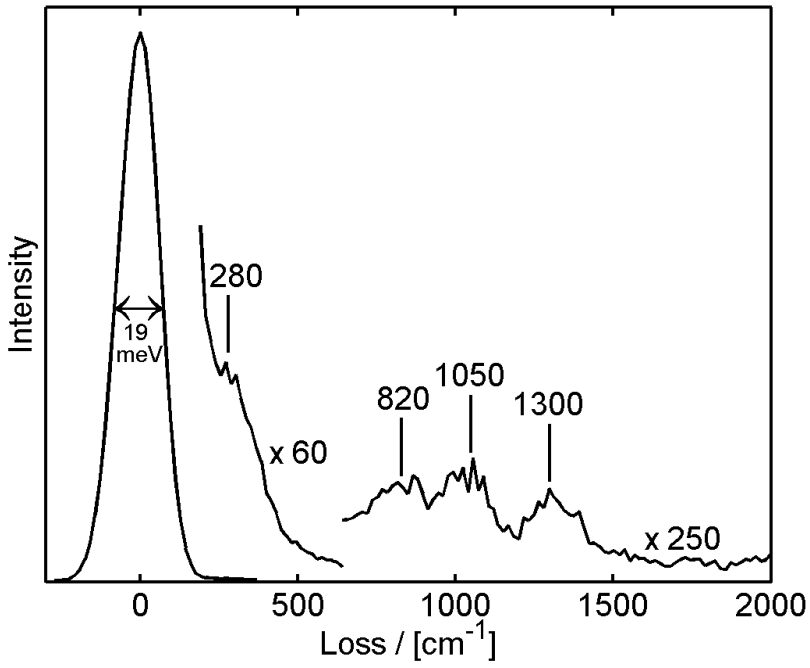

Figure 9. EELS spectrum taken after the high pressure experiment on 1 ML Cu. A primary energy of 8 eV was used, and the resolution was 19 meV. Peaks are observed at approx. 280, 820, 1050, and 1300 cm^{-1}.

The binding and vibrational states of the carbonate species were examined further on several Cu and Pt systems utilizing DFT calculations. It was observed that CO_3 binds as a bidentate species to all (111) surfaces and through all three oxygen atoms at steps on (211) surfaces, with the exception of Pt(211). Monodentate binding geometries were probed through the calculations but those states were not stable. On Cu exposing (111) surfaces the two binding O atoms always prefer bridge positions, whereas on Pt-exposing (111) surfaces the O atoms always prefer on-top sites. On the alloyed Cu/Pt overlayer on Pt (111), CO_3 showed hybrid binding to a Pt-top and a Cu-Cu bridge site.

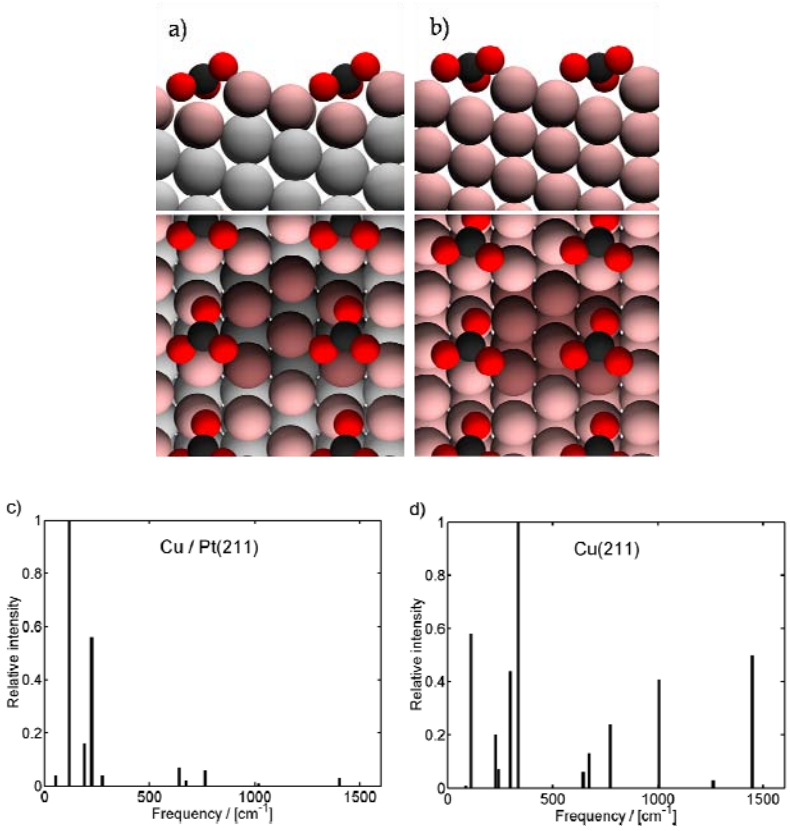

Figure 10. Upper panels: Carbonate adsorbed on (a) Cu/Pt(211) and (b) Cu(211) as seen in cross-section and a top view. The unit cell region is shaded dark. Lower panels (c) and (d) show the calculated relative intensities for all 3*N* vibrational modes (including the frustrated rotational and translational modes on the surface) of the carbonate on Cu/Pt(211) and Cu(211), respectively, both projected onto the direction perpendicular to the (111) facets. The intensities are estimated based upon the relative dipole change and depend on the direction of projection as on the adsorbate orientation. Some modes listed in Table 4 may not be visible due to very low intensities.

Table 4. Comparison of DFT and spectroscopic results for vibrational frequencies in cm-1. Only experimentally observed modes and the corresponding calculated frequencies are shown.

Mode	Observed EELS/IR Cu/Pt(111)	DFT, Stepped Surfaces				DFT, Flat Surfaces				
		Cu(211)	Pt(211)	1 ML Cu on Pt(211)	Pt-Cu-Pt(211)	Cu(111)	Pt(111)	1 ML Cu on Pt(111)	Pt-Cu-Pt(111)	Cu/Pt on Pt(111)
ν_a(OCO)[a]	1310/ 1435-1410	1447/ 1262	1163	1282/ 1402	1201/ 1448	969	1222	969	1242	1134
ν_s(OCO)[a]			946			891	961	892	974	878
ν(CO)[b]	1050	1004	1634	1021	989	1759	1629	1742	1611	1688
π(CO3)	820	773	733	751	757	768	710	768	721	749
ν(M-O)	280	299/ 245	342	284/ 309	342/ 300/ 148	281/ 236	314/ 278	301/ 215/ 174	309	309/ 220

[a] For the tridentate CO_3 it is difficult to make a clear distinction between the symmetric and asymmetric (O-C-O) stretches.

[b] For the tridentate CO_3 ν(CO) is a star vibration where all three O atoms vibrate simultaneously.

With the exception of pure Pt, it is found that CO_3 binds almost flat at the step on all (211) surfaces, see Figure 10(a) and (b). On Pt(211) top-top binding on two step atoms is observed, *i.e.*, a bidentate configuration. For all systems studied, CO_3 states adsorbed on steps are generally 0.5 to 0.7 eV more stable than on flat terraces, which indicate that steps should be the preferred adsorption sites. Only the systems with tridentate CO_3 lying flat on a (211) step site exhibit similar frequencies as observed in the EELS spectrum, see Table 4. None of the bidentate configurations on the studied (111) surfaces as well as Pt(211), exhibit CO_3 vibrational spectra in any reasonable agreement between theory and experiments. For the tridentate configurations at steps the most intense predicted peaks are at low wave numbers, see Figure 10(c) and (d), whereas for bidentate configurations the most intense peaks are around 1800 cm^{-1}. No peaks around 1800 cm^{-1} were observed either in UHV or high-pressure experiments and, furthermore, the most intense peaks are observed at low energies, which upon comparison with DFT also confirm that CO_3 should be located at steps/defects. This leads to the conclusion that CO_3 prefers to adsorb to steps or step defects based on the considerably enhanced binding energy and the close match between the observed and calculated frequencies at these sites.

We find that all three O atoms of CO_3 interact with the metal surface atoms when adsorbed on steps, and as a result, it is difficult to directly compare to literature assignments which are for monodentate or bidentate species, as the vibrational modes are different in the tridentate case. In particular, the calculated ν(CO) mode is a CO_3 "star" vibration, where all three O

atoms vibrate simultaneously. Furthermore, it is in some cases hard to clearly distinguish between a symmetric vs. asymmetric (O-C-O) stretch on, for example, Cu/Pt(211). That is probably because of the high degree of asymmetry characteristic of CO_3 when bound to the step.

It is speculated that higher pressures lead to higher CO_3 coverage and increased adsorbate-adsorbate repulsion. CO_3 may be destabilized and slightly raised from the surface causing the angle between the molecular plane and the z-axis perpendicular to the surface to change. Hence, the intensities of modes within the molecular plane may be significantly altered leading to the observation of the O=C=O stretch. As pressure decreases, the interaction energy is decreased, and the carbonate settles down to a point where only the weak 1310 cm^{-1} stretch can be distinguished. It has not been possible to assign the 1205 cm^{-1} high pressure mode. It is most likely some type of O-C-O stretch.

It was not always possible to detect the carbonate with vibrational methods. Certain conditions had to be met in order to get a signal in the spectra. For instance, a high CO_2 pressure had to be applied immediately, as slow inlet in stages of 10 mbar yielded a high oxygen coverage which in effect poisoned the surface. This reduced the amount of carbonate produced significantly. Furthermore, an increase in the amount of deposited Cu above 2 ML made it very difficult to detect the carbonate, although it was later observed with TPD and XPS, as presented in the next section.

Similar high pressure experiments were also done on the pristine Pt(111) surface as a blank sample and on a surface alloy corresponding to a Cu/Pt ratio of 1:2, which was produced from 1 ML Cu by annealing the sample briefly at 573 K. Neither of these samples showed any features in PM-IRRAS or EELS spectra except for small amounts of adsorbed CO.

3.3.3 TPD and XPS Studies

After the spectroscopic examinations of the adsorbed species formed during exposure to 0.5 bar CO_2 at room temperature, TPD and XPS were employed to study the decomposition of the carbonate and to estimate the coverage.

TPD spectra were recorded in the 300-600 K range with a heating rate of β = 2 K/s for samples with different amounts of Cu dosed at 425 K on the platinum crystal, as well as a Cu/Pt surface alloy. Spectra for mass 28 and 44 are shown in Figure 11(a) and (b) together with 0.5 ML CO adsorbed on the clean Pt(111) crystal as a reference. No hydrogen was observed during any of the experiments, and the maximum temperature employed was kept low enough to avoid desorption of the surface oxygen.

The 1:2 Cu/Pt surface alloy did not promote a dissociation of CO_2 or formation of carbonate, but instead adsorbed CO from the background pressure of the chamber. According to the TPD spectrum, Figure 11(a), CO is bound more weakly on the alloy compared to Pt(111). This agrees with prior observations in literature where CO TPDs reveal a lowering of the desorption peak maximum by approx. 100 K [47]. A very weak CO_2 feature is visible in the TPD spectrum for the alloy, Figure 11(b), but it is most likely due to small patches of unalloyed Cu on Pt.

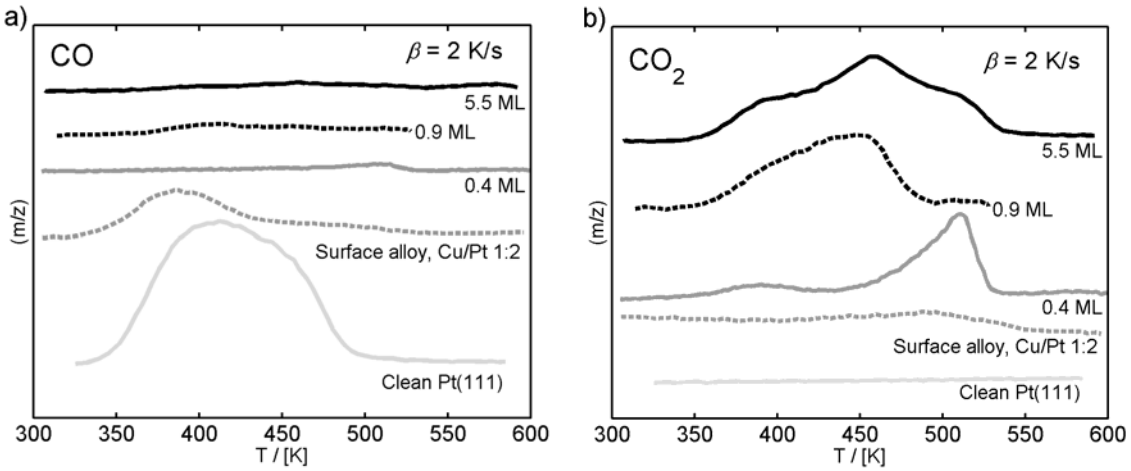

Figure 11. TPD spectra of (a) CO - mass 28, and (b) CO_2 - mass 44 after exposure to 0.5 bar CO_2. The surfaces examined were 0.4, 0.9, and 5.5 ML Cu deposited at 425 K and a Cu:Pt = 1:2 surface alloy produced by flashing 1 ML Cu on Pt to 573 K. The pure Pt crystal predosed with 0.5 ML CO at room temperature is shown for comparison. The temperature ramp was β = 2 K/s.

For 0.4 ML Cu which should correspond to a pseudomorphic stretched Cu layer with a low degree of island formation, no CO and H_2 were observed. Moreover, two CO_2 features, a very weak and broad feature at 390 K and a large and sharp feature at 510 K with a shoulder toward lower temperature, emerged, see Figure 11(b). At 0.9 ML where second layer Cu islands have formed, these features had merged leading to one broad feature with a maximum at 450 K, and for even higher Cu coverages where Cu(111) bulk properties are expected to return [48], a more complicated CO_2 spectrum was obtained, probably due to a highly defective surface with extensive island growth. At these Cu coverages, the desorption feature had broadened further spanning a 180 K range consisting of a main peak at 460 K with both high and low temperature shoulders. The explanation of the complicated carbonate decomposition pattern is not easy, since the feature above 460 K is undoubtedly connected to the onset of surface alloying. As such, that feature might not be related to the magnitude of the binding energy, but rather to the surface reconstruction.

Table 5. Binding energy for the 1s oxygen core-level in eV for CO_3, CO_2, CO, and O adsorbed on Pt reported by Norton [71], Ni by Behm and Brundle [72], and Cs-Cu(110) by Carley *et al.* [18] compared to results from the present study.

Species	$E_{binding}$ (Pt) [71]	$E_{binding}$ (Ni) [72]	$E_{binding}$ Cs-Cu(110) [18]	$E_{binding}$ (This work)
CO_2	534.5	-	536	-
CO	532.7		533	533.0
CO_3	-	531.2	531	531.1
O	530.2	-	529.8	530.0

It is also seen that the amount of carbonate on 5.5 ML Cu is comparable to the amount produced on 0.9 ML. Combined with the poor detection of the carbonate through the vibrational spectroscopies, it suggests a somewhat different arrangement of the carbonate at high pressures on the multilayered Cu/Pt(111) system compared to the 0.9 ML Cu/Pt(111) system, although a possible decrease of the signal due to surface roughness should also be considered. XPS spectra of the O 1s region, Figure 12(a), and the C 1s region, Figure 12(b), for the 1 ML Cu/Pt(111) system were recorded before and after TPD. An oxygen peak was initially observed at a binding energy of 531 eV. The area was calibrated with a 0.5 ML CO reference, and it was established that the oxygen peak corresponded to a coverage of approx. 0.9 ML, or 0.3 ML CO_3. In the carbon region a peak was observed at 289 eV with an area corresponding to 0.2 ML. This is in accordance with the ratio expected for carbonate when taking experimental uncertainties into account. Moreover, the carbon peak had disappeared and one third of the adsorbed oxygen was left on the surface after decomposition of the carbonate during TPD, supporting the decomposition step

$$CO_3^* \rightarrow CO_2\,(g) + O^*$$

where * denotes an adsorption site. O 1s XPS binding energies for adsorbed C_xO_y-species have been examined on Pt by Norton [71], on Ni by Behm and Brundle [72], and on Cu(110) promoted with Cs and oxygen [18]. A comparison to the results from this work is found in Table 5. The O 1s XPS binding energies of the different species agree very well. Throughout the experiments it was found that the Cu 2p peaks were not affected by exposure to CO_2.

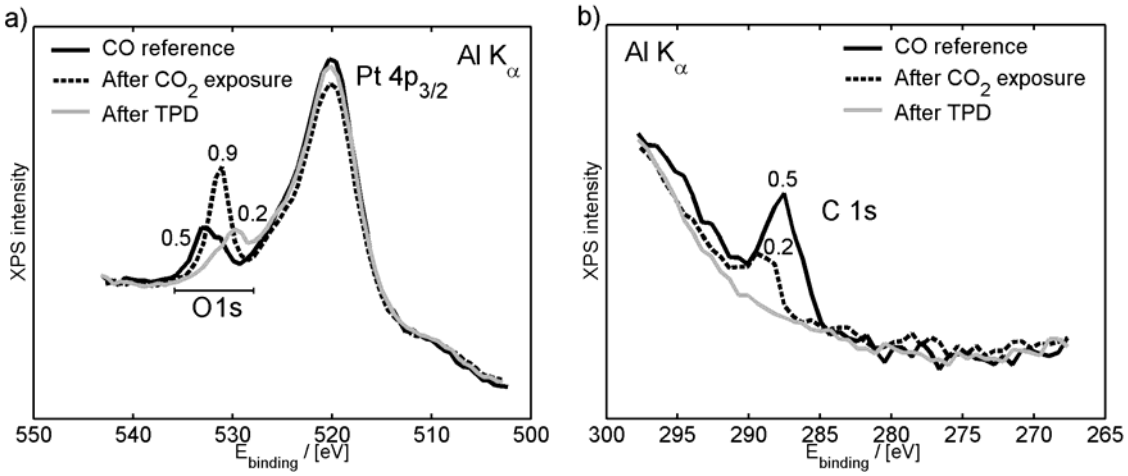

Figure 12. XPS spectra for (a) oxygen 1s and platinum $4p_{3/2}$, and (b) carbon 1s before and after TPD on 1 ML Cu/Pt(111). The spectrum for 0.5 ML CO is shown as a reference.

3.3.4. Effect of Predosed Oxygen

Several groups have shown that a pre-existing oxygen coverage influence the amount of carbonate that may be formed during CO_2 exposure [34, 73]. To investigate the effect on the present system, 6 L oxygen corresponding to an 0.15 ML coverage on 0.9 ML Cu/Pt(111) were dosed before high pressure CO_2 exposure at room temperature. No differences in PM-IRRAS or subsequent XPS and TPD spectra could be observed compared to initially oxygen-free Cu-layers. At 0.3 ML oxygen the carbonate formation reaction was inhibited as previously observed for polycrystalline Cu [34], and for low coverages of pre-adsorbed oxygen the missing oxygen needed for the equilibrium amount of adsorbed CO_3 was formed by dissociation of CO_2 during high pressure exposure.

To elucidate the reaction mechanism isotope experiments were also conducted. Predosing 6 L $^{18}O_2$ and subsequent exposure to 0.5 bar of CO_2 for approx. 30 minutes led to a total exchange of the surface oxygen. No isotopes (mass 46 for $C^{16}O^{18}O$, and mass 48 for $C^{18}O_2$) were detected in TPD above normal levels for the gas used. Furthermore, only ^{16}O was left on the surface after TPD, when checked with ISS, which allows for a clear distinction between ^{16}O and ^{18}O [74]. Thus, at high pressure the surface oxygen exchange process is highly dynamic.

Formation of carbonate under UHV conditions was also examined, as predosed oxygen is needed to produce carbonate on Ag in this situation [75]. 2000 L CO_2 were dosed at room temperature with the ion gauge turned off to avoid dissociation of CO_2. It was observed that

carbonate in small amounts could be formed on 1 ML Cu when 6 L $^{18}O_2$ had been predosed, and both masses 44 and 46 were observed in TPD spectra. ISS subsequently only detected ^{16}O, revealing an asymmetry in the carbonate formation vs. decomposition pathway. A blank experiment without predosed oxygen was also performed, and as expected no carbonate could be formed in UHV under these conditions.

3.4 Summary

Evidence has been presented for the dissociation of CO_2 and subsequent formation of a stable carbonate species on Cu/Pt(111) when the surface is subjected to a high pressure of CO_2 at room temperature. PM-IRRAS spectra show a pressure dependence of the vibrational spectra which is interpreted as a shift in position of the carbonate. Subsequent EELS spectra in UHV yield states that are consistent with a configuration lying nearly flat on the surface. DFT calculations suggest steps and defects as the most likely carbonate adsorption sites, where CO_3 appears to be more stable than on terrace sites by 0.5-0.7 eV. Furthermore, the calculations yield frequencies close to those observed for stepped surfaces, and their intensities are in reasonable agreement with experiments. Decomposition of the carbonate is seen over a wide temperature range in TPD, with the main peak around 450 K for 0.9 ML Cu. Furthermore, XPS suggests that approximately one third of the adsorbed oxygen is left on the surface after TPD, corresponding to the expected ratio for carbonate decomposition.

It has been found that dissociation of CO_2 occurs at high pressure, which evidently leads to the formation of a stable carbonate species. In addition, it was observed that, under UHV conditions, small amounts of preadsorbed atomic oxygen significantly decrease the activation barrier for carbonate formation. The formation of carbonate must then be initiated by dissociation of CO_2 through the following sequence of elementary steps, where * denotes a surface site.

$$CO_2\,(g) + * \rightarrow CO_2*$$

$$CO_2* \rightarrow CO(g) + O*$$

$$CO_2* + O* \rightarrow CO_3* + *$$

For methanol synthesis catalysts there are several studies that have speculated or observed that a carbonate species is involved in the reaction steps on high index and rough Cu surfaces [15, 18, 34, 35]. Waugh suggested a reaction mechanism, where the formation of a transient carbonate and subsequent hydrogenation to formate (HCOO) explained the activation of CO_2 and H_2 [76]. This has been observed experimentally by Millar *et al.* on Cu/SiO_2 [68]. It thus seems that the key step in methanol synthesis is the activation of CO_2 through a carbonate intermediate and this activation is necessary to form formate.

4. OVERALL CONCLUSIONS

Process Design Analysis

We presented two process designs for the production of methanol from H_2/CO_2 and H_2O/CO. The two alternatives can be integrated with thermochemical processes for the splitting of H_2O and/or CO_2, leading to technologies that can change the way we view renewable energy. The integrated processes satisfy the twofold objective of fomenting the use of renewable energy (in this case concentrated solar power) while reducing CO_2 emissions trough recycling. Simulations of the proposed alternatives feature methanol yields significantly better than those reported in the literature. Based upon current methanol prices, sensitivity analysis indicates economic feasibility, if prices do not exceed 1.12 USD/kgH_2 (7.88 USD/GJ) and 0.17 USD/kgCO. However, even if the cost is twice as high, the processes can be economically attractive if the price of methanol increases moderately.

DFT Study of Methanol Synthesis from CO_2 and H_2 mixtures

On the basis of our previous DFT calculations on the Cu(111) surface we developed a microkinetic model for methanol synthesis from mixtures of $CO/CO_2/H_2$. Several reaction pathways were included and no assumptions about the mechanism or the rate determining step were made. The model was then fitted to published kinetic data obtained from experiments using a commercial $Cu/ZnO/Al_2O_3$ catalyst. Our model indicates that, depending on feed composition and pressure/temperature conditions, a significant fraction of the MeOH produced is synthesized from CO_2 via the intermediates HCOO, HCOOH, CH_3O_2, CH_2O, and CH_3O. The remaining MeOH is synthesized along the route CO, HCO, CH_2O, and CH_3O. In order to obtain a good fit, the binding energies of OH, CO_2, HCO, HCOOH, CH_3O_2, CH_2O, CH_3OH had to be increased, indicating that the Cu(111) surface may not be the most reactive facet on the real catalyst. The adjusted binding energies suggest that the active site is either a more open or stepped Cu surface or the Cu surface may be partially oxidized. Two mechanisms that could explain CO promotion were considered in our model: (a) removal of OH via COOH to form CO_2 + H and (b) CO assisted hydrogenation of intermediates formed in the CO_2 reaction path via HCO. Both mechanisms show only minor contributions to the overall reaction and the main effect of CO appears to be the additional MeOH production by CO hydrogenation.

5. REFERENCES

1. Smith, O.H., R. Friedman, and J.C. Venter, *Biological solutions to renewable energy.* National Academy of Engineering website: http://www.nae.edu/nae/bridgecom.nsf/BridgePrintView/MKUF-5NTMX9?OpenDocument.
2. Dukes, J.S., *Burning Buried Sunshine: Human Consumption of Ancient Solar Energy.* Climatic Change, 2003. **61**: p. 31.
3. Zhu, X.-G., S.P. Long, and D.R. Ort, *What is the Maximum Efficiency with Which Photosynthesis Can Convert Solar Energy into Biomass?* Biotechnology, 2008. **19**: p. 153.
4. Diver, R.B., et al., *Solar Thermochemical Water-splitting Ferrite-cycle Heat Engines.* Journal of Solar Energy Engineering, 2008. **130**(4): p. 041001.
5. Miller, J.E., et al., *Metal oxide composites and structures for ultra-high temperature solar thermochemical cycles.* J. Mater. Sci., 2008. **43**: p. 4714-4728.
6. Joo, O.S. and K.D. Jung, *CAMERE Process for Methanol Synthesis from CO2 Hydrogenation.* Carbon Dioxide Utilization for Global Sustainability, 2004. **153**: p. 67.
7. Mignard, D., et al., *Methanol Synthesis From Flue-Gas CO2 and Renewable Electricity: a Feasibility Study.* Int. J. Hydrogen Energy, 2003. **28**: p. 455.
8. Rasmussen, P.B., et al., *Methanol Synthesis on Cu(100) from a Binary Gas-Mixture of CO_2 and H_2.* Catalysis Letters, 1994. **26**(3-4): p. 373-381.
9. Kagan, Y.B., et al., *Mechanism of Synthesis of Menthol from Carbon-Dioxide and Hydrogen.* Doklady Akademii Nauk SSSR, 1975. **221**(5): p. 1093-1095.
10. Chinchen, G.C., et al., *Mechanism of Methanol Synthesis from $CO_2/CO/H_2$ Mixtures over Copper/Zinc Oxide/Alumina Catalysts - Use of C^{14}-Labeled Reactants.* Applied Catalysis, 1987. **30**(2): p. 333-338.
11. Chinchen, G.C., et al., *Synthesis of Methanol .1. Catalysts and Kinetics.* Applied Catalysis, 1988. **36**(1-2): p. 1-65.
12. Solymosi, F., *The Bonding, Structure and Reactions of CO_2 Adsorbed on Clean and Promoted Metal-Surfaces.* Journal of Molecular Catalysis, 1991. **65**(3): p. 337-358.
13. Freund, H.J. and M.W. Roberts, *Surface chemistry of carbon dioxide.* Surface Science Reports, 1996. **25**(8): p. 225-273.
14. Fu, S.S. and G.A. Somorjai, *Interactions of O_2, CO, CO_2, and D_2 with the Stepped Cu(311) Crystal-Face - Comparison to Cu(110).* Surface Science, 1992. **262**(1-2): p. 68-76.
15. Bönicke, I.A., W. Kirstein, and F. Thieme, *A Study on CO_2 Dissociation on a Stepped (332) Copper Surface.* Surface Science, 1994. **309**: p. 177-181.
16. Rodriguez, J.A., W.D. Clendening, and C.T. Campbell, *Adsorption of CO and CO_2 on Clean and Cesium-Covered Cu(110).* Journal of Physical Chemistry, 1989. **93**(13): p. 5238-5248.
17. Thomsen, E.V., B. Jørgensen, and J. Onsgaard, *Adsorption and Reactivity of CO_2 on the K/Cu(110) Interface and the Effect of Photon Irradiation.* Surface Science, 1994. **304**(1-2): p. 85-97.

18. Carley, A.F., M.W. Roberts, and A.J. Strutt, *Activation of Carbon-Monoxide and Carbon-Dioxide at Cesium-Promoted Cu(110) and Cu(110)-O Surfaces.* Journal of Physical Chemistry, 1994. **98**(37): p. 9175-9181.
19. Habraken, F.H.P.M., E.P. Kieffer, and G.A. Bootsma, *Study of the Kinetics of the Interactions of O_2 and N_2O with a Cu(111) Surface and of the Reaction of Co with Adsorbed Oxygen Using AES, LEED and Ellipsometry.* Surface Science, 1979. **83**(1): p. 45-59.
20. Campbell, C.T., K.A. Daube, and J.M. White, *Cu/ZnO(000-1) and ZnOx/Cu(111) - Model Catalysts for Methanol Synthesis.* Surface Science, 1987. **182**(3): p. 458-476.
21. Krause, J., D. Borgmann, and G. Wedler, *Photoelectron spectroscopic study of the adsorption of carbon dioxide on Cu(110) and Cu(110)/K - As compared with the systems Fe(110)/CO_2 and Fe(110)/K+CO_2.* Surface Science, 1996. **347**(1-2): p. 1-10.
22. Ernst, K.H., D. Schlatterbeck, and K. Christmann, *Adsorption of carbon dioxide on Cu(110) and on hydrogen and oxygen covered Cu(110) surfaces.* Physical Chemistry Chemical Physics, 1999. **1**(17): p. 4105-4112.
23. Funk, S., et al., *Adsorption dynamics of CO_2 on Cu(110): A molecular beam study.* Surface Science, 2006. **600**(3): p. 583-590.
24. Wachs, I.E. and R.J. Madix, *Selective Oxidation of CH_3OH to H_2CO on a Copper(110) Catalyst.* Journal of Catalysis, 1978. **53**(2): p. 208-227.
25. Schneider, T. and W. Hirschwald, *Interaction of Carbon-Dioxide with Clean and Oxygenated Cu(110) Surfaces.* Catalysis Letters, 1992. **14**(2): p. 197-205.
26. Campbell, C.T., *Interaction of Carbon-Dioxide with Clean and Oxygenated Cu(110) Surfaces - Comment.* Catalysis Letters, 1992. **16**(4): p. 455-457.
27. Schneider, T. and W. Hirschwald, *Interaction of Carbon-Dioxide with Clean and Oxygenated Cu(110) Surfaces - Response.* Catalysis Letters, 1992. **16**(4): p. 459-460.
28. Rasmussen, P.B., P.A. Taylor, and I. Chorkendorff, *The Interaction of Carbon-Dioxide with Cu(100).* Surface Science, 1992. **270**: p. 352-359.
29. Nakamura, J., J.A. Rodriguez, and C.T. Campbell, *Does CO_2 Dissociatively Adsorb on Cu Surfaces.* Journal of Physics: Condensed Matter, 1989. **1**: p. Sb149-Sb160.
30. Copperthwaite, R.G., et al., *The reactive chemisorption of carbon dioxide at magnesium and copper surfaces at low temperature.* Catalysis Letters, 1988. **1**(1): p. 11-19.
31. Hadden, R.A., et al., *The adsorption and decomposition of carbon dioxide on polycrystalline copper.* Catalysis Letters, 1988. **1**(1): p. 27-33.
32. Haas, T. and J. Pritchard, *Adsorption of Carbon-Dioxide on Polycrystalline Copper.* Journal of the Chemical Society, Faraday Transactions, 1990. **86**(10): p. 1889-1892.
33. Browne, V.M., et al., *Activation of Carbon-Dioxide at Bismuth, Gold and Copper Surfaces.* Applied Surface Science, 1991. **47**(4): p. 375-379.
34. Carley, A.F., et al., *Surface oxygen and chemical specificity at copper and caesium surfaces.* Faraday Discussions, 1996: p. 225-235.
35. Chinchen, G.C., et al., *Promotion of Methanol Synthesis and the Water-Gas Shift Reactions by Adsorbed Oxygen on Supported Copper-Catalysts.* Journal of the Chemical Society, Faraday Transactions, 1987. **83**: p. 2193-2212.
36. Chinchen, G.C., K. Mansfield, and M.S. Spencer, *The Methanol Synthesis - How Does It Work.* Chemtech, 1990. **20**(11): p. 692-699.

37. Topsøe, N.-Y. and H. Topsøe, *FTIR studies of dynamic surface structural changes in Cu-based methanol synthesis catalysts.* Journal of Molecular Catalysis A: Chemical, 1999. **141**(1-3): p. 95-105.
38. Greeley, J., et al., *CO vibrational frequencies on methanol synthesis catalysts: a DFT study.* Journal of Catalysis, 2003. **213**(1): p. 63-72.
39. Schumacher, N., et al., *Trends in low-temperature water-gas shift reactivity on transition metals.* Journal of Catalysis, 2005. **229**(2): p. 265-275.
40. Rodriguez, J.A. and M. Kuhn, *Electronic-Properties and Chemical-Properties of Ag/Pt(111) and Cu/Pt(111) Surfaces - Importance of Changes in the D-Electron Populations.* Journal of Physical Chemistry, 1994. **98**(44): p. 11251-11255.
41. Ruban, A., et al., *Surface electronic structure and reactivity of transition and noble metals.* Journal of Molecular Catalysis A: Chemical, 1997. **115**(3): p. 421-429.
42. Mavrikakis, M., B. Hammer, and J.K. Nørskov, *Effect of strain on the reactivity of metal surfaces.* Physical Review Letters, 1998. **81**(13): p. 2819-2822.
43. Hammer, B. and J.K. Nørskov, *Theoretical surface science and catalysis - Calculations and concepts.* Advances in Catalysis, 2000. **45**: p. 71-129.
44. Greeley, J., J.K. Nørskov, and M. Mavrikakis, *Electronic Structure and Catalysis on Metal Surfaces.* Annual Review of Physical Chemistry, 2002. **53**: p. 319-348.
45. Shek, M.L., et al., *Photoemission-Study of the Adsorption of Cu on Pt(111).* Physical Review B, 1983. **27**(12): p. 7277-7287.
46. Shek, M.L., et al., *CO Chemisorption on Cu Adlayers on Pt(111).* Physical Review B, 1983. **27**(12): p. 7301-7312.
47. Yeates, R.C. and G.A. Somorjai, *The growth and alloy formation of copper on the platinum (111) and stepped (553) crystal surfaces; characterization by LEED, AES, and CO thermal desorption.* Surface Science, 1983. **134**(3): p. 729-744.
48. Paffett, M.T., et al., *Cu Adsorption on Pt(111) and Its Effects on Chemisorption - a Comparison with Electrochemistry.* Surface Science, 1985. **154**(1): p. 284-302.
49. Rodriguez, J.A., C.M. Truong, and D.W. Goodman, *Infrared Vibrational Studies of Co Adsorption on Cu/Pt(111) and Cupt(111) Surfaces.* Journal of Chemical Physics, 1992. **96**(10): p. 7814-7825.
50. Nohlen, M., M. Schmidt, and K. Wandelt, *On the Influence of Adsorbates on Heteroepitaxy - Work Function Oscillations during Deposition of Copper on Platinum(111).* Surface Science, 1995. **333**: p. 902-907.
51. Kolodzejczyk, M., et al., *Interaction between Cu and Pt(111) in the reaction $CO+O_2$ modification by Cu sub-monolayers and cooperation between pure and Cu-modified Pt(111).* Applied Surface Science, 1997. **121**: p. 480-483.
52. Holst, B., et al., *The growth of ultra thin Cu-films on Pt(111), probed by helium atom scattering and scanning tunnelling microscopy.* Surface Science, 1997. **377**(1-3): p. 891-894.
53. Holst, B., et al., *Observation of an adlayer-driven substrate reconstruction in Cu-Pt(111).* Physical Review B, 1998. **58**(16): p. R10195-R10198.
54. Tsay, J.S., et al., *Comparative study of annealing effects for Cu/Pt(111) films with and without oxygen.* Surface Science, 2001. **482**: p. 866-871.
55. Tsay, J.S., et al., *Adsorption of oxygen on ultrathin Cu/Pt(111) films.* Journal of Vacuum Science & Technology, A: Vacuum, Surfaces, and Films, 2001. **19**(5): p. 2217-2221.

56. Tsay, J.S., T. Mangen, and K. Wandelt, *Kinetic study of the formation of a surface-confined $Cu_{50}Pt_{50}$ alloy.* Thin Solid Films, 2001. **397**(1-2): p. 152-156.
57. Canzian, A., H.O. Mosca, and G. Bozzolo, *Atomistic modeling of Pt deposition on Cu(111) and Cu deposition on Pt(111).* Surface Review and Letters, 2004. **11**(2): p. 235-243.
58. Knudsen, J., et al., *A Cu/Pt near-surface alloy for water-gas shift catalysis.* Journal of the American Chemical Society, 2007. **129**(20): p. 6485-6490.
59. MacLaren, D.A., et al., *Submonolayer alloying of copper on vicinal platinum: A combined atom and ion scattering study.* Physical Review B, 2004. **70**(12): p. -.
60. Leung, L.W.H., T.W. Gregg, and D.W. Goodman, *Electrochemical and Ultrahigh-Vacuum Characterization of Ultrathin Cu Films on Pt(111).* Langmuir, 1991. **7**(12): p. 3205-3210.
61. Taylor, P.A., et al., *Formate Synthesis on Cu(100).* Surface Science, 1992. **261**(1-3): p. 191-206.
62. Johansson, M., J.H. Jørgensen, and I. Chorkendorff, *Combined high-pressure cell-ultrahigh vacuum system for fast testing of model metal alloy catalysts using scanning mass spectrometry.* Review of Scientific Instruments, 2004. **75**(6): p. 2082-2093.
63. Buffeteau, T., B. Desbat, and J.M. Turlet, *Polarization Modulation Ft-Ir Spectroscopy of Surfaces and Ultra-Thin Films - Experimental Procedure and Quantitative-Analysis.* Applied Spectroscopy, 1991. **45**(3): p. 380-389.
64. Green, M.J., B.J. Barner, and R.M. Corn, *Real-Time Sampling Electronics for Double Modulation Experiments with Fourier-Transform Infrared Spectrometers.* Review of Scientific Instruments, 1991. **62**(6): p. 1426-1430.
65. Barner, B.J., et al., *Polarization Modulation Fourier-Transform Infrared Reflectance Measurements of Thin-Films and Monolayers at Metal-Surfaces Utilizing Real-Time Sampling Electronics.* Analytical Chemistry, 1991. **63**(1): p. 55-60.
66. Hammer, B., L.B. Hansen, and J.K. Nørskov, *Improved adsorption energetics within density-functional theory using revised Perdew-Burke-Ernzerhof functionals.* Physical Review B, 1999. **59**: p. 7413.
67. Greeley, J. and M. Mavrikakis, *A first-principles study of surface and subsurface H on and in Ni(111): diffusional properties and coverage-dependent behavior.* Surface Science, 2003. **540**(2-3): p. 215-229.
68. Millar, G.J., et al., *A Combined Infrared, Temperature Programmed Desorption and Temperature Programmed Reaction Spectroscopy Study of CO_2 and H_2 Interactions on Reduced and Oxidized Silica-Supported Copper-Catalysts.* Molecular Physics, 1992. **76**(4): p. 833-849.
69. Stuve, E.M., R.J. Madix, and B.A. Sexton, *An EELS Study of CO_2 and CO_3 Adsorbed on Oxygen Covered Ag(110).* Chemical Physics Letters, 1982. **89**(1): p. 48-53.
70. Herzberg, G., *Infrared and Raman spectra of polyatomic molecules*. Molecular spectra and molecular structure. Vol. 2. 1945, New York: Van Nostrand, Reinhold.
71. Norton, P.R., *Surface Analysis of Platinum by X-Ray Photoelectron-Spectroscopy (XPS).* Surface Science, 1974. **44**(2): p. 624-628.
72. Behm, R.J. and C.R. Brundle, *On the Formation and Bonding of a Surface Carbonate on Ni(100).* Surface Science, 1991. **255**(3): p. 327-343.
73. Barteau, M.A. and R.J. Madix, *Lateral Interaction Effects on the Reaction of CO_2 and Oxygen Adsorbed on Ag(110).* Journal of Chemical Physics, 1981. **74**(7): p. 4144-4149.

74. Andersen, M. 2005, Technical University of Denmark: Copenhagen, Denmark.
75. Bowker, M., M.A. Barteau, and R.J. Madix, *Oxygen Induced Adsorption and Reaction of H_2, H_2O, CO and CO_2 on Single-Crystal Ag(110).* Surface Science, 1980. **92**(2-3): p. 528-548.
76. Waugh, K.C., *The absorption and locking-in of hydrogen in copper.* Solid State Ionics, 2004. **168**(3-4): p. 327-342.

DISTRIBUTION

1	MS0887	Duane B. Dimos	1800
5	MS1349	Richard A. Kemp	1815
1	MS1349	William F. Hammetter	1815
1	MS1349	James E. Miller	1815
1	MS1349	Constantine A. Stewart	1815
1	MS0899	Technical Library	9536 (electronic copy)
1	MS0123	D. Chavez, LDRD Office	1011


Sandia National Laboratories